

Localization of spherical photoacoustic sources in acrylamide gels using time domain measurements

J. A. Viator and G. Paltauf^b and S. L. Jacques^a and S. A. Prahl^a

Oregon Medical Laser Center, Portland, OR

Oregon Graduate Institute of Science and Technology, Portland, OR

Oregon Health Sciences University, Portland, OR^a

Institut für Experimentalphysik, Karl-Franzens-Universität, Graz, Austria^b

ABSTRACT

Photoacoustic imaging may be used to detect tumor masses in biological tissue. In particular, time of flight measurements of the photoacoustic waves may indicate tumor location. Here we use time of flight information to localize spherical photoacoustic sources in tissue phantoms. A Q-switched, frequency-doubled Nd:YAG laser operating at 532 nm with a pulse duration of 5 ns irradiated absorbing spheres 2 mm in diameter. The spheres were in mineral oil or turbid acrylamide blocks. A PVDF acoustic transducer was built and used to detect the acoustic waves. The position of the detector was translated so that the time of flight information from two acoustic waveforms from the source could be correlated by a convolution algorithm. This convolution resulted in a two dimensional map indicating the position of the source. Source location was indicated to within 5% of the true location for acoustic propagation distances of 20 mm. An image source is also indicated when the true source was in proximity to a reflecting boundary.

Keywords: photoacoustics, time of flight, acrylamide, Nd:YAG, acoustic, PVDF, spherical source

1. INTRODUCTION

Photoacoustic methods have been used to obtain information about optical properties of laser irradiated targets [1–4]. The optical contrast between a hypervascular mass, such as a tumor, and surrounding tissue, such as fatty tissue may allow the generation of photoacoustic waves that can be used to localize the hypervascular mass. Analysis of the acoustic wave, particularly with respect to time of flight, may be used to determine the location, size, and optical properties of the photoacoustic source. Such information may be used for tumor imaging. This paper offers an experimental set up and a simple computational algorithm that localizes the photoacoustic source.

There are several ways in which laser light can be converted into acoustic radiation [5]. This paper investigates only the photothermal effect of a stress confined laser pulse resulting in a thermoelastic expansion. This thermoelastic expansion gives rise to an acoustic wave. A laser pulse can be considered stress confined if the pulse duration is shorter than the time required for the energy to acoustically radiate away from the region of optical absorption. This can be represented by the equation [1, 3, 4]

$$\tau < \frac{\delta}{c_s} \quad (1)$$

where τ is the pulse duration of the laser, δ is the absorption depth, and c_s is the speed of sound in the medium. The condition of stress confinement is met in the experiments described in this paper as the pulse duration of the laser was 5 ns, the speed of sound in the media is 1.5 mm/mms and the absorption coefficient of the absorbing sphere was 60 cm^{-1} .

For an absorption coefficient of 60 cm^{-1} , a 2 mm sphere is not optically thin, meaning the absorption of optical energy is not homogeneous throughout the volume of the sphere. The absorption depth for a 60 cm^{-1} sphere is approximately $300 \mu\text{m}$, thus the region of absorption in the sphere is a cap, as shown in figure 1. As the spheres were

Direct correspondence to S.A.P, prahl@ece.ogi.edu; (503) 216–2197; <http://omlc.ogi.edu/>

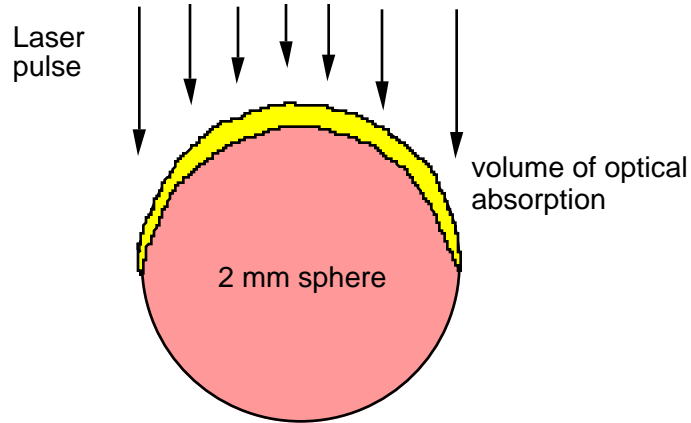


Figure 1. The absorption of optical radiation in an optically thick sphere occurs in the spherical cap closest to the direction of the laser pulse.

not optically thin, the convolution algorithm localized the spherical cap source, with the highest amplitude occurring with the acoustic wave peak. This peak corresponded to the central point of the surface of the cap, where absorption was the highest and no tensile stresses would interfere with the signal.

In these experiments spheres were irradiated with laser energy giving rise to photoacoustic waves. The waves were detected and analyzed with respect to time of flight data. The analysis resulted in localization of the spheres, recognizing the fact, as noted above, that the sources were not spherical with respect to acoustic generation. The analysis, using linear convolution of the data, resulted in a 2-D map of the source location. The irradiated sphere was localized to within 5% of their true positions, as indicated on the convolution map. The sphere also created an image source, due to the proximity of a reflecting boundary caused by the air/phantom interface at the phantom surface. The source was approximately 4 mm from the surface, creating an image 8 mm away, which was indicated in the convolution map.

2. MATERIALS AND METHODS

2.1. Set Up

The photoacoustic setup is shown in figure 2. A Q-switched, frequency-doubled Nd:YAG laser operating at 532 nm with a pulse duration of 5 ns was used to irradiate tissue phantoms. The phantoms were either a turbid acrylamide block or a cuvette with mineral oil. The phantoms contained a 2 mm optically absorbing acrylamide sphere. The laser pulse was coupled into a 1000 μm fiber. The output of the fiber was imaged onto the target via a biconvex lens with a focal length of 19 mm. The resultant laser spot was 3.3 mm in diameter with a pulse energy of 5.6 mJ. This gave a radiant exposure of 0.066 J/cm². The laser pulse, being stress confined, created a photoacoustic wave which propagated through the phantom and was detected by a piezoelectric transducer. The acoustic wave was then sent to a digital storage oscilloscope (DSA 602A, Tektronics, Wilsonville, OR).

For the initial sphere detection scheme, a sphere was placed 15 mm above the detection plane, so that the detector was 15 mm directly below the bottom of the sphere. Thus, the acoustic signal was generated approximately 17 mm above the detector. The sphere was immersed in mineral oil. For the actual time of flight experiments, the sphere was placed 18 mm above the detector plane, directly above the detector active area. Thus the acoustic signal was generated approximately 20 mm above the detector plane. The transducer was translated 6 mm laterally for the second detection point.

2.2. Acoustic Transducer

We built an acoustic transducer with a polyvinylidene fluoride (PVDF) piezoelectric element (figure 3). The PVDF film was coated on both sides with aluminum, which was etched with FeCl₃ to form the active area. The active area

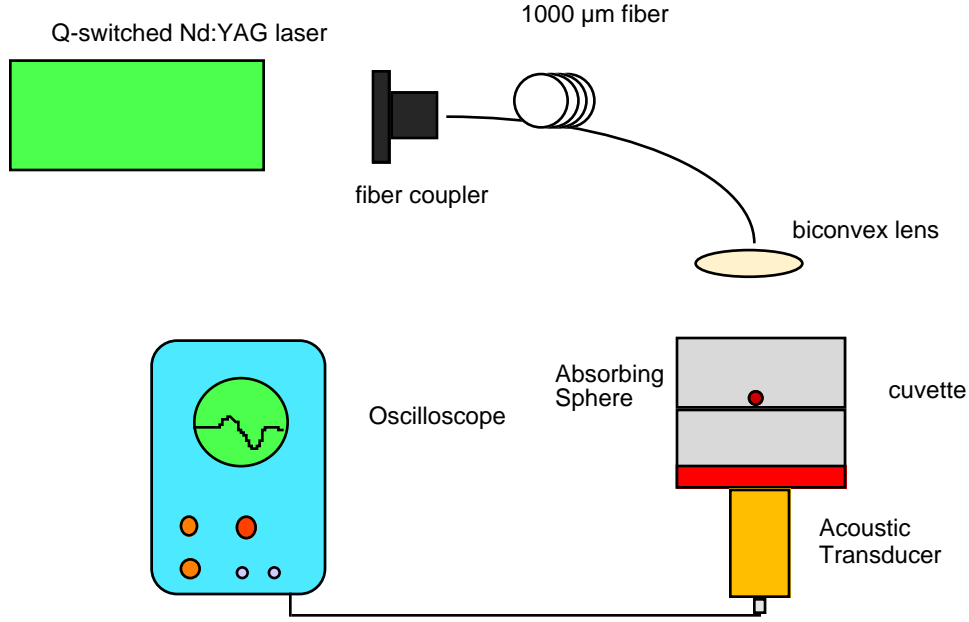


Figure 2. The photoacoustic experimental set up. The Nd:YAG laser pulse was coupled into a 1000 μm fiber. The fiber face was imaged onto the target. A PVDF transducer was used to detect the resultant acoustic waves. The waveform was then sent to a digital oscilloscope.

was in the form of two crossed aluminum electrodes. The PVDF active area was 1.8 mm by 1.8 mm and placed on a cylindrical plug of acrylic. The acrylic plug served as a base for the sensing element and was housed in a brass cylinder. The negative and positive electrodes were connected to a BNC connector.

The transducer sensitivity was calibrated using absorbing solutions made from Direct Red 81 (Sigma Chemical) and deionized water. The solutions were purely absorbing and had absorption coefficients of 26, 54, 102, and 151 cm^{-1} as determined with a spectrophotometer (Hewlett Packard, 8452A Diode Array Spectrophotometer). The calibration setup is shown in figure 2, with an absorbing Direct Red 81 solution used instead of an absorbing sphere. The Nd:YAG laser described above was coupled to the 1000 μm optical fiber and the fiber face was imaged onto the surface of the Direct Red solutions by a biconvex lens. The spot on the surface was 3.3 mm in diameter. The energy of the laser pulse was 5.6 J, giving a radiant exposure of 0.066 J/cm^2 . The pressure of the resulting acoustic wave was calculated using [3, 4]

$$p_0(z) = \mu_a \Gamma H_0 \exp(-\mu_a z) \quad (2)$$

where Γ is the unitless Grüneisen coefficient. The value $\Gamma = 0.12$ was used [1]. The Grüneisen coefficient describes the fraction of optical energy that is translated into thermoelastic expansion. The depth in the medium is given by z . H_0 is the incident laser radiant exposure. For $z = 0$, the pressure can be calculated and the corresponding voltage on the acoustic peak will indicate the transducer calibration factor in mV/bar.

2.3. Acrylamide Gels

Tissue phantoms were made with acrylamide gels. Acrylamide gels were used to create small spheres with Direct Red 81 (Sigma Chemical) as an absorber. The sizes of the spheres were 2 mm with $\mu_a = 60 \text{ cm}^{-1}$. These spheres were placed in turbid acrylamide blocks and in mineral oil (Mineral Oil, Fleet Pharmaceuticals, Lynchburg, VA), then irradiated with the laser to create acoustic waves.

The acrylamide was made according to the procedure outlined by Sathyam *et al.* [6] and Viator *et al.* [4]. 9.735 g of acrylamide and 0.265 g of bis-acrylamide (Sigma Chemical) were dissolved in 50 ml of deionized water to form a 20% polyacrylamide gel. Polymerization was induced by adding an initiator of 0.02 g of ammonium persulfate and



Figure 3. The acoustic transducer was a PVDF film detector in a brass housing. A BNC was connected to the PVDF electrodes for coupling to the oscilloscope. The active area is shown as the crossed region on the top of the transducer.

0.2 ml of TEMED (Sigma Chemical). For the turbid blocks, a 1:20 dilution of intralipid in deionized water (Liposyn II, Abbott Laboratories, North Chicago, IL) was used instead of pure deionized water.

The absorbing spheres were made by injecting small quantities of acrylamide solution into heated mineral oil. The acrylamide had been initiated, so that the spherical drops of acrylamide in the mineral oil would gel. The oil was heated to 80° C to accelerate the gelling process. The amount of injected acrylamide solution determined the size of the spheres. Three small spheres are shown in figure 4.

2.4. Convolution Algorithm

A convolution algorithm was written in Mathematica. The algorithm is expressed as a simple convolution product

$$M(x, y) = W(t_1) \otimes W(t_2) \quad (3)$$

where $M(x, y)$ is the two dimensional convolution map that indicates the source location. Higher values of $M(x, y)$ correspond to higher certainties of source location. $W(t_i)$ is the i^{th} acoustic waveform, normalized by the maximum value of $W(t_i)$. The linear convolution product is given by \otimes . The convolution takes each point of the first acoustic waveform and correlates its value with each point of the second waveform. Alternatively, the relation between the convolution map and the waveforms can be described as operations on the x and z coordinates

$$M(x, y) = W\left(\frac{1}{c}\sqrt{x^2 + z^2}\right) \cdot W\left(\frac{1}{c}\sqrt{(x-d)^2 + z^2}\right) \quad (4)$$

where the multiplication is carried through for x and z , the lateral and vertical distances, respectively. The transducer translation distance is denoted as d . A typical convolution map as a density plot is shown in figure 5. In this case,

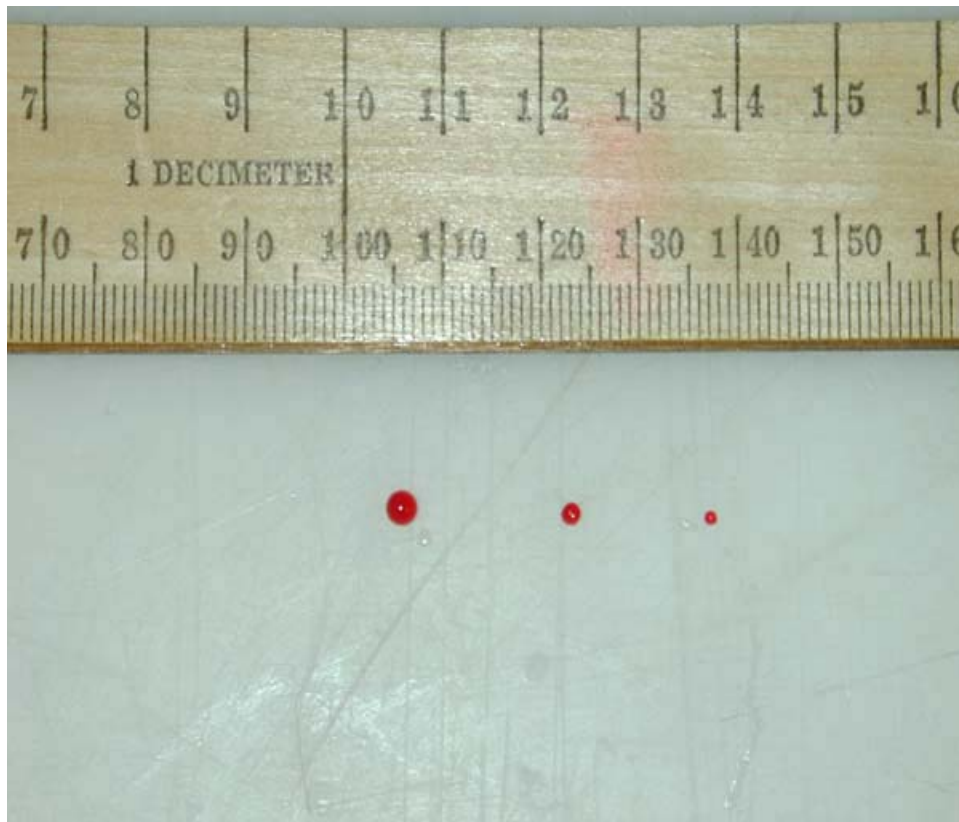


Figure 4. Three acrylamide spheres are shown here. The sizes are 3 mm, 2 mm, and 1 mm as shown from left to right.

a turbid acrylamide block containing an absorbing sphere was irradiated by the laser, creating an acoustic wave detected by the PVDF transducer. The transducer was translated and a second waveform was detected. The waveforms were convolved, producing the map. The backprojection arcs are visible in the density plot. The source was placed directly above the first transducer position at a distance of 5 mm. The density plot indicated the source location by the single bright spot at the intersection of the arcs. The source was indicated at a distance of 5 mm, offset to the side by about 1 mm.

3. RESULTS

3.1. Transducer Calibration

The calibration curve for the transducer sensitivity is shown in figure 6. The transducer sensitivity was 12.6 ± 0.8 mV/bar over the range of absorption coefficients of the Direct Red solutions. This result was applicable to the absorption coefficient of the spheres, being 60 cm^{-1} .

3.2. Acoustic Waveform from Optically Thick Spheres

A photoacoustic waveform for a 2 mm sphere is shown in figure 7. In this case, the sphere was directly above the detector at a distance of 15 mm. The negative peak corresponding to the center of the spherical cap was detected at $11.5 \mu\text{s}$, indicating a distance of 17.25 mm. Since the actual source was the top cap of the sphere, this corresponded to the correct propagation time of the acoustic wave. The waveform is similar to the computer simulation for a 60 cm^{-1} , 2 mm sphere positioned 15 mm from the detector (figure 8).

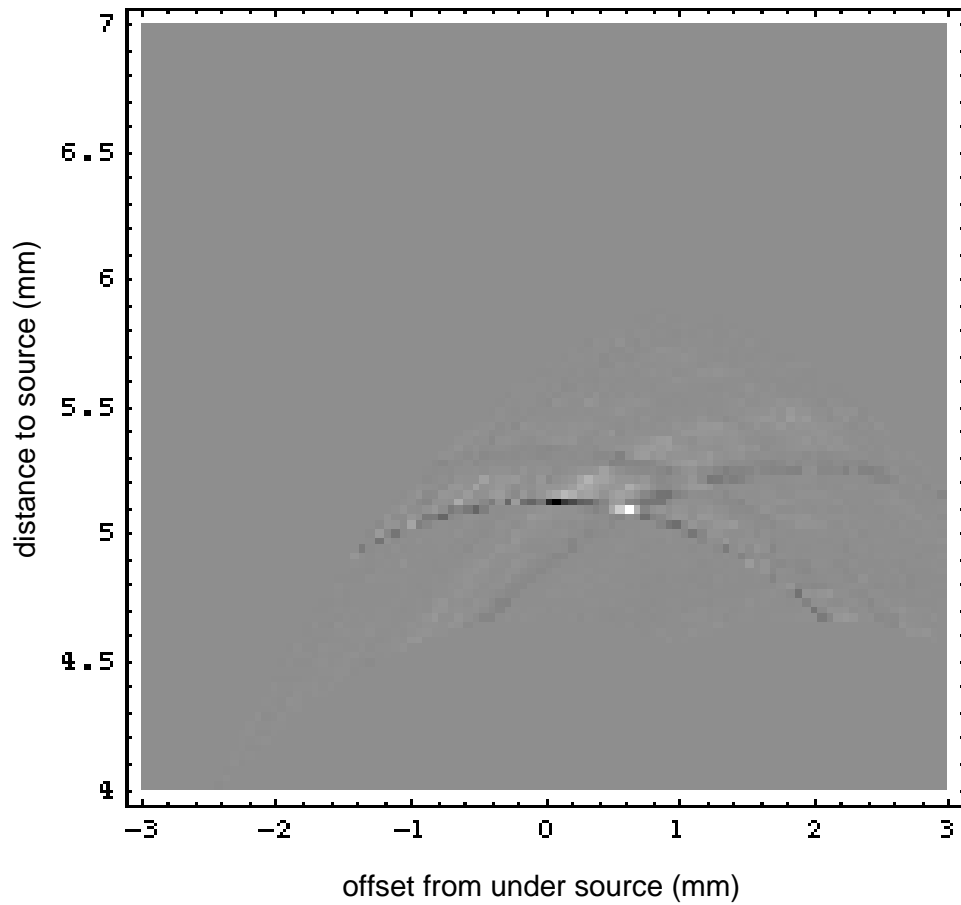


Figure 5. This is a density plot of the location of an absorbing acrylamide sphere in a turbid acrylamide block. The bright spot at the intersection of the backprojection arcs indicates the predicted position of the photoacoustic source. The vertical axis shows the distance above the initial transducer location (5 mm), while the horizontal axis shows the lateral offset of the sphere from the transducer (0.5 mm). The true position was 5 mm above and 0 mm offset.

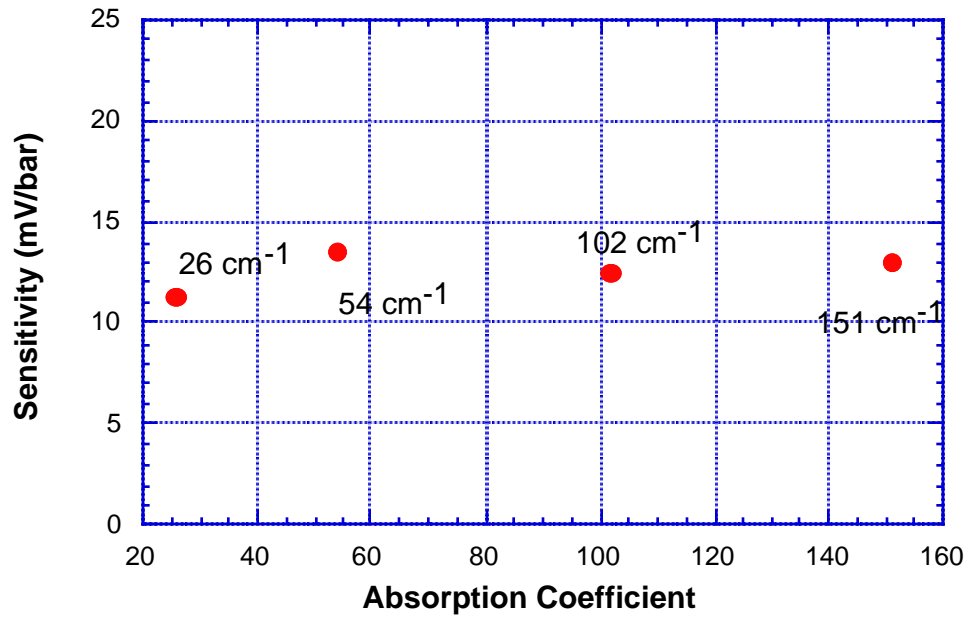


Figure 6. This is the calibration curve for the PVDF transducer. The calibration was done for 26, 54, 102, and 151 cm^{-1} Direct Red 81 solutions. The calibration was approximately 12.6 ± 0.8 mV/bar.

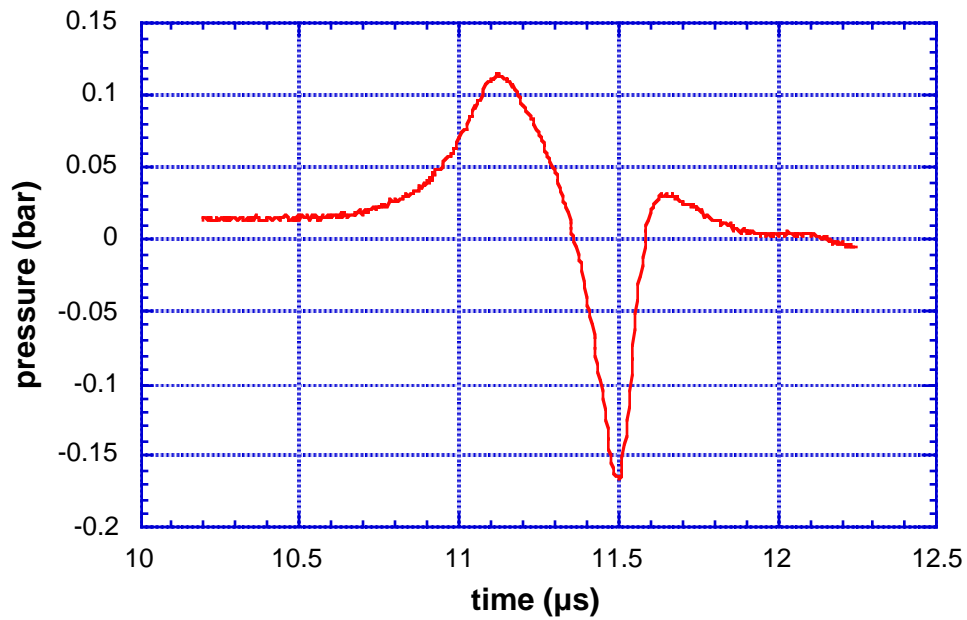


Figure 7. This is the waveform from irradiating an optically thick sphere (60 cm^{-1}) with a 2 mm diameter 15 mm directly above the PVDF transducer. The sphere was immersed in mineral oil.

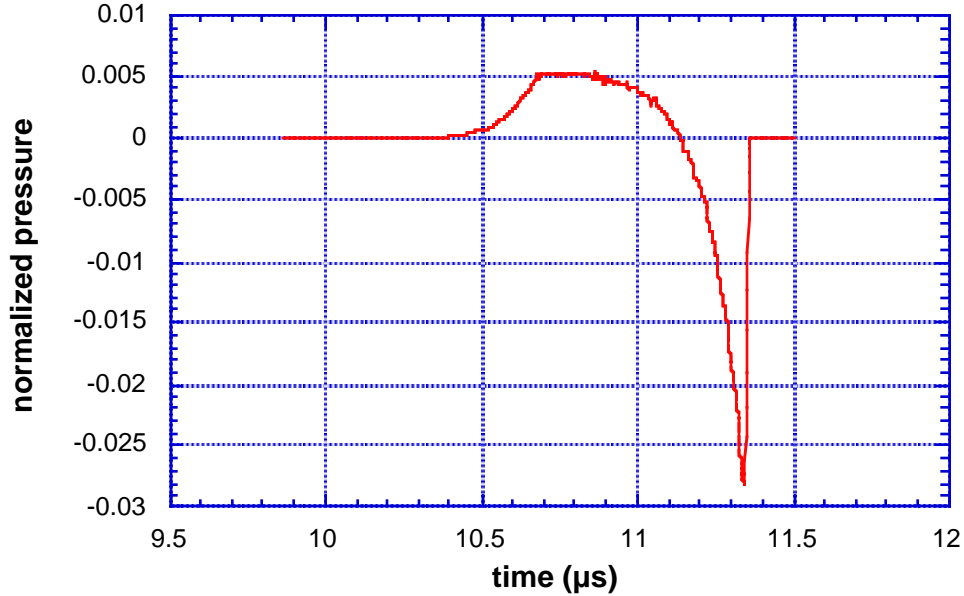


Figure 8. A simulation of a 60 cm^{-1} , 2 mm sphere irradiated by a stress confined laser pulse. The sphere was centered 15 mm above the detector.

3.3. Localization of Spherical Sources

Two acoustic waveforms from the photoacoustic source are shown in figure 9. In each graph, the first waveform is the initial acoustic wave detected by the PVDF transducer. The second waveform is a reflection from the surface of the tissue phantom. This image source was included in the convolution algorithm. The three dimensional rendering of the convolution map of the acoustic waveforms is shown in figure 10. The map indicates that the sphere position was directly above the initial detector position at a distance of 21 mm. The true position was 20 mm, since the sphere was 2 mm in diameter and the distance from the bottom of the sphere to the detector was 18 mm. The prediction was within 5% of the true value. The image source was 8 mm above that, outside the tissue phantom, clearly indicating a virtual source.

4. DISCUSSION

Photoacoustic imaging has been studied recently with some success. Jacques *et al.* [8] and Andersen *et al.* [9] used optical detection schemes to find buried absorbers using photoacoustic methods. Liu offered theoretical investigations into photoacoustic imaging using the Radon transform and the P-transform [10,11]. Esenaliev *et al.* [7] performed experiments to find the detection limit of tumor phantoms in gels and chicken breast tissue. They detected signals from 2 mm spheres in gelatin at a distance of 60 mm. They also detected small pieces of liver buried in chicken breast tissue at a distance of 80 mm. This paper attempts similar detection using purely time of flight information to detect optically absorbing spheres in tissue phantoms. The eventual goal is to localize tumors and determine size and optical properties.

The sphere detected as shown in figure 7 is similar to the simulation in figure 8. The arrival time of the simulation is $11.35\ \mu\text{s}$, corresponding to the correct propagation distance of 17 mm, which was the distance from the detector to the top of the sphere, the source of the acoustic energy. The arrival time of the waveform in the experiment was $11.5\ \mu\text{s}$. This later arrival was probably due to the sphere being slightly larger than 2 mm. A measurement error of only $200\ \mu\text{m}$ would account for this deviation. More importantly, the duration of the pulse in the simulation is longer, indicating a bigger sphere. This can be explained by a smaller absorption volume of the sphere in the experiment due to optical index of refraction mismatch between the acrylamide sphere and the mineral oil it was embedded in. The index of refraction for mineral oil is 1.471, while the index for acrylamide is 1.367. This difference causes a

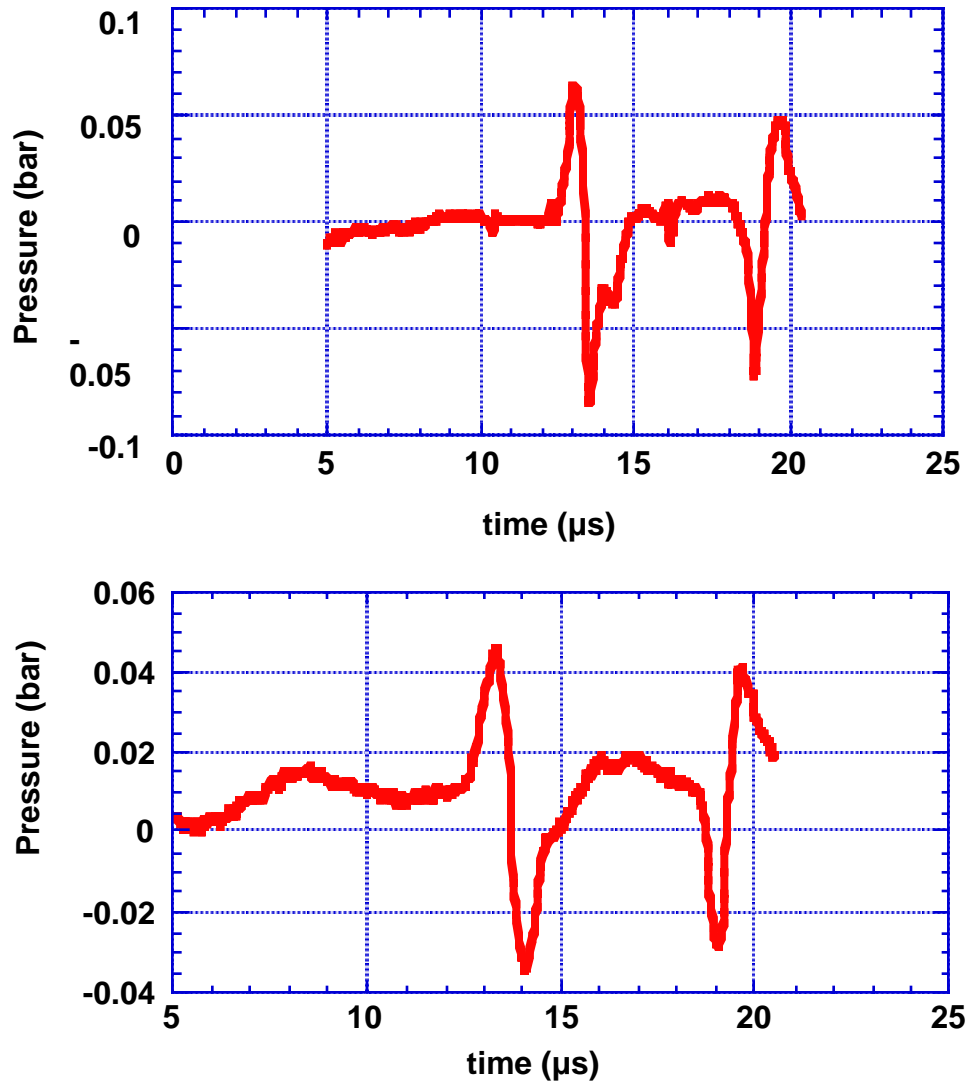


Figure 9. The two waveforms used for the convolution algorithm are shown here. The first waveform (top) was from the initial detector position. The second waveform (bottom) was from the detector translated 6 mm laterally. The first peak on both waveforms was from the actual sphere. The second peak on both waveforms was from the acoustic reflection from the acrylamide surface.

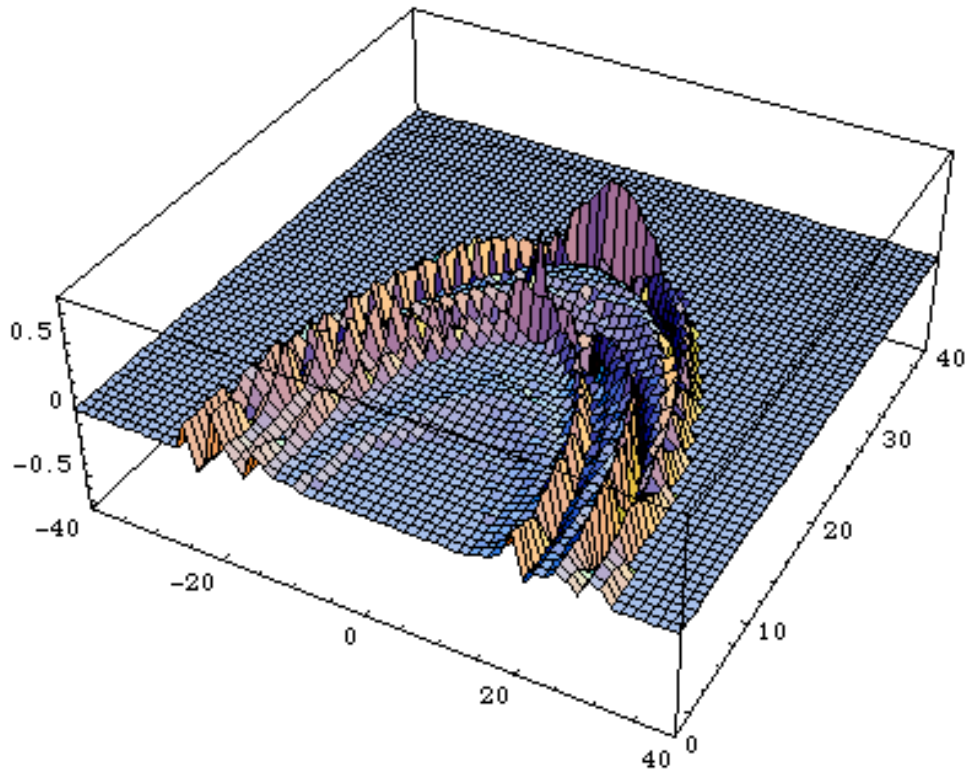


Figure 10. This is a 3-D graphic indicating the position of the spherical source as predicted by the convolution algorithm.

reflection on the surface of the sphere near the equator, preventing absorption from happening, creating a smaller volume of optical absorption. A simple geometric analysis shows that the critical angle truncates the outer $400\ \mu\text{m}$ of the sphere, making the sphere look $800\ \mu\text{m}$ smaller in diameter.

Similar geometric analysis of the photoacoustic wave may give sphere size information. This information, in conjunction with information about absorbed energy, may even shed light on the optical absorption of the sphere.

The convolution algorithm succeeded in localizing the photoacoustic source to within 5% of the true position. This algorithm may have the advantage over traditional backprojection in that it correlates every point on the original detected waveform with every point on waveform from the laterally translated detector. The value of each point may be considered a probability, as the waveforms are normalized. The result is a correlation of probabilities, accounting for multiple source and acoustic wave structure.

The convolution algorithm will be later tested for more complicated boundary conditions and multiple sources. Minimum distances to resolve multiple source, including image sources, will be determined, thus leading to an eventual imaging scheme for buried optical absorbers when combined with the size and optical property determinations mentioned above.

REFERENCES

1. A. A. Oraevsky, S. L. Jacques, and F. K. Tittel, "Mechanism of laser ablation for aqueous media irradiated under stress confined conditions," *J. Appl. Phys.* **78**, pp. 1281–1289, 1995.
2. S. L. Jacques, "Laser-tissue interactions. Photochemical, photothermal and photomechanical," *Lasers General Surg.* **72**, pp. 531–557, 1992.
3. G. Paltauf, H. Schmidt-Kloiber, and H. Guss, "Light distribution measurements in absorbing materials by optical detection of laser-induced stress waves," *Appl. Phys. Lett.* **69**, pp. 1526–1528, 1996.

4. J. A. Viator, S. L. Jacques, and S. A. Prahl, "Depth profiling of absorbing soft materials using photoacoustic methods," *IEEE J. Selected Topics Quantum Electron.* **5**, pp. 989–996, 1999.
5. M. W. Sigrist, "Laser generation of acoustic waves in liquids and gases," *J. Appl. Phys.* **60**, pp. R83–121, 1986.
6. U. S. Sathyam and S. A. Prahl, "Limitations in measurements of subsurface temperatures using pulsed photothermal radiometry," *J. Biomed. Opt.* **2**, pp. 251–261, 1997.
7. R. O. Esenaliev, A. A. Karabutov, and A. A. Oraevsky, "Sensitivity of laser opto–acoustic imaging in detection of small deeply embedded tumors," *IEEE J. Selected Topics Quantum Electron.* **5**, pp. 981–988, 1999.
8. S. L. Jacques, P. E. Andersen, S. G. Hanson, and L. R. Lindvold, "Non–contact detection of laser–induced acoustic waves from buried absorbing objects using a dual–beam common–path interferometer," *SPIE Proc.* **3254**, pp. 307–318, 1998.
9. P. E. Andersen, S. G. Hanson, and S. L. Jacques, "Photoacoustic imaging of buried objects using an all–optical detection scheme," *SPIE Proc.* **3601**, pp. 303–309, 1999.
10. P. Liu, "Image reconstruction from photoacoustic pressure signals," *SPIE Proc.* **2681**, pp. 285–296, 1996.
11. P. Liu, "The p–transform and photoacoustic image reconstruction," *Phys. Med. Biol.* **43**, pp. 667–674, 1998.